Soft chemical control of the crystal and magnetic structure of a layered mixed valent manganite oxide sulfide

Jack N. Blandy, Artem M. Abakumov, Kirsten E. Christensen, Joke Hadermann, Paul Adamson, Simon J. Cassidy, Silvia Ramos, David G. Free, Harry Cohen, Daniel N. Woodruff, Amber L. Thompson, and Simon J. Clarke

Citation: APL Materials **3**, 041520 (2015); doi: 10.1063/1.4918973
View online: http://dx.doi.org/10.1063/1.4918973
View Table of Contents: http://scitation.aip.org/content/aip/journal/aplmater/3/4?ver=pdfcov
Published by the AIP Publishing

Soft chemical control of the crystal and magnetic structure of a layered mixed valent manganite oxide sulfide

Jack N. Blandy,[1,2] Artem M. Abakumov,[3] Kirsten E. Christensen,[1] Joke Hadermann,[3] Paul Adamson,[1] Simon J. Cassidy,[1,2] Silvia Ramos,[4] David G. Free,[1] Harry Cohen,[1] Daniel N. Woodruff,[1] Amber L. Thompson,[1] and Simon J. Clarke[1]

[1]*Inorganic Chemistry Laboratory, Department of Chemistry, University of Oxford, South Parks Road, Oxford OX1 3QR, United Kingdom*
[2]*Diamond Light Source Ltd., Harwell Science and Innovation Campus, Didcot OX11 0DE, United Kingdom*
[3]*Electron Microscopy for Materials Science (EMAT), University of Antwerp, Groenenborgerlaan 171, B-2020 Antwerp, Belgium*
[4]*School of Physical Sciences, Ingram Building, University of Kent, Canterbury, Kent CT2 7NH, United Kingdom*

(Received 18 March 2015; accepted 13 April 2015; published online 21 April 2015)

Oxidative deintercalation of copper ions from the sulfide layers of the layered mixed-valent manganite oxide sulfide $Sr_2MnO_2Cu_{1.5}S_2$ results in control of the copper-vacancy modulated superstructure and the ordered arrangement of magnetic moments carried by the manganese ions. This soft chemistry enables control of the structures and properties of these complex materials which complement mixed-valent perovskite and perovskite-related transition metal oxides. [http://dx.doi.org/10.1063/1.4918973]

Layered oxide chalcogenides are a class of compound in which oxide layers containing relatively electropositive metal ions (e.g., lanthanide or early-to-mid transition metal ions) are separated by chalcogenide layers containing relatively electronegative metal ions (e.g., coinage metal ions). Some of these compounds such as LaCu*Ch*O and related materials are of interest as transparent conducting materials because the sulfide-3*p*-dominated valence band can readily accept holes. Electron doping may also be performed. This area has been extensively reviewed.[1] More complex oxide chalcogenides[2] contain a redox-active transition metal ion in the oxide layer. The ordering of oxide and chalcogenide ions results in anisotropic coordination environments for the transition metal ions and we have previously described how control of the ligand field anisotropy results in control of the orbital contribution to the ordered magnetic moment in the Co^{II} series $(Sr_{1-x}Ba_x)_2CoO_2Cu_2S_2$ with the structure type depicted in the inset to Figure 1.[3] In the series $Sr_2MnO_2\,Cu_{2m-\delta}S_{m+1}$ (m = 1–3),[4,5] a deficiency of $\delta = 0.5$ Cu(I) ions on the tetrahedral sites in the copper sulfide antifluorite-type layers goes hand in hand with a mean Mn oxidation state of +2.5. Mn is in an unusual axially distended MnO_4S_2 octahedral coordination environment with the MnO_4 squares vertex linked to form MnO_2 sheets. These mixed-valent manganite oxide sulfides complement the many perovskite, brownmillerite, or Ruddlesden-Popper manganites with oxidation states around +3.5 which show exotic interplay of crystal structure, transport properties, and magnetism. Indeed in the isoelectronic $Mn^{+2.5}$ series $Sr_2MnO_2Cu_{1.5}(S_{1-x}Se_x)_2$, we have revealed[6] an interplay between magnetically ordered states that is strikingly similar to that offered by perovskite and Ruddlesden-Popper $Mn^{+3.5}$ oxide manganites, despite the different electron counts and ligand fields.

Here, we explore the topotactic oxidative deintercalation chemistry of $Sr_2MnO_2Cu_{1.5}S_2$ at around ambient temperatures to synthesize metastable compositions with a larger copper deficiency and describe some of the resulting changes in crystal structure and magnetic properties. This soft chemistry is enabled by the high copper ion mobility in these materials which is common when Cu(I) ions are coordinated by polarizable anions. This mobility results in the onset of long range

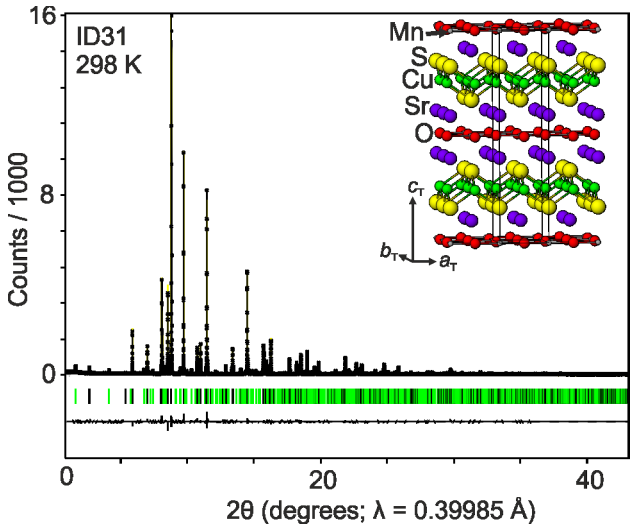

FIG. 1. Rietveld refinement against ID31 data (λ = 0.4 Å) for the modulated crystal structure of $Sr_2MnO_2Cu_{1.3}S_2$. Green reflection markers indicate reflections arising from the modulation. The idealized crystal structure for its parent $Sr_2MnO_2Cu_{1.5}S_2$ is shown in the inset.

copper/vacancy order below room temperature[6] and also enables a reductive and topotactic lithiation in which copper is completely extruded from the material and replaced by lithium using chemical or electrochemical methods.[7,8]

$Sr_2MnO_2Cu_{1.5}S_2$ powder was prepared as described previously[5,6] by reacting stoichiometric amounts of SrS, MnO_2, and Cu powders at 900 °C for 24 h in an alumina crucible contained within a dried, evacuated silica tube. Single crystals of sufficient size for X-ray diffraction investigations may routinely be extracted from the products of these syntheses.[5] The deintercalation was performed by the reaction, under anaerobic conditions, of a suspension of the powder with a 0.015M solution of iodine in dry acetonitrile solution for between 1 and 7 days at 0 °C. After the reaction, the solid was washed with dry acetonitrile, filtered, dried under vacuum, and handled in an argon-filled glove box. The oxidized products were found to be subject to aerial decomposition. Structural characterization of the products was performed using: X-ray powder diffraction (XRPD) on the high resolution powder diffractometer ID31 at the ESRF, Grenoble, France; X-ray single crystal diffraction (XRSCD) on I19 (Experimental Hutch 1) at the Diamond Light Source, UK; Neutron powder diffraction (NPD) on D2B at the ILL, Grenoble, France and Scanning Transmission Electron Microscopy (STEM) using a FEI Titan at EMAT, Antwerp. Single crystal and Rietveld analyses were carried out using the JANA2006 software.[9] Mn and Cu *K*-edge X-ray absorption spectra were obtained in transmission mode on B18 at Diamond and were calibrated against metal foils. Magnetometry used a Quantum Design MPMS-XL instrument.

Oxidation of $Sr_2MnO_2Cu_{1.5}S_2$ produced crystalline products with lattice parameters shortened by up to 0.45% in the basal directions and up to 0.7% perpendicular to the layers. Control of the reaction time enabled products with a range of lattice parameters to be obtained. Reactions carried out at room temperature were found to result in smaller contractions of the unit cells than those performed at 0 °C, despite the consumption of iodine being greater in the ambient temperature reactions. This was found to be a consequence of side-reactions with iodine competing with the deintercalation of copper which make the chemical determination of composition by measuring iodine consumption unreliable. The oxidized samples decomposed on gentle annealing (up to 500 °C), with the re-formation of the parent phase ($Sr_2MnO_2Cu_{1.5}S_2$) and the production of corresponding impurities (SrS and MnO were identified from XRPD).[10] The oxidized compounds also decomposed on exposure to moist air or moist argon at ambient temperatures, although they were quite resistant to decomposition under exposure to dry O_2.[10] Stronger oxidizing agents (NO_2BF_4 and Br_2, both in MeCN) were found to produce complete decomposition of the oxide sulfide phase.

The reflections of the $Sr_2MnO_2Cu_{1.5}S_2$ parent compound (cell volume 276.9 Å^3 for two formula units) were retained on deintercalation to form the $Sr_2MnO_2Cu_{1.5-x}S_2$ products and the room temperature evolution of the cell volume of this body-centred tetragonal cell with changing copper content are shown as supplementary material (Figure S1).[11] Analysis of room temperature XRPD data revealed a phase gap between unit cell volumes of 273.8 Å^3 and 272.8 Å^3 which is the minimum cell volume obtained by oxidation using I_2 in the manner described. Some samples were found to be composed of two phases with diffraction peaks readily resolved using ID31 (see Figure S2[11]). There was no observable splitting of the main Bragg reflections that could not be accounted for by phase separation around a phase gap, but additional weak reflections were clearly evident in the laboratory and synchrotron XRPD patterns for the more highly oxidized materials on the copper-poor side of the phase gap with the smaller unit cells. We describe the crystal structure and properties of this most highly oxidized material obtained from the reaction with iodine in some detail in this article. The detailed evolution of structure and properties over the entire range of available intermediate compositions and as a function of temperature will be presented elsewhere.

A preliminary description of the structure of the most highly oxidized material was initially accomplished on a single large batch of sample using electron diffraction and imaging and synchrotron X-ray powder diffraction. This sample was large enough for neutron powder diffraction. The analysis of electron diffraction data and data from ID31 on this sample revealed that the additional weak Bragg reflections could be accounted for by a structural modulation indexed with a (3 + 1)D approach which may be summarized as follows: in the $Cu_{1.5-x}S_2$ block, a longitudinal displacive modulation of Cu ion positions is superimposed on an occupational modulation of the Cu site. In the oxide layer, by contrast, the Sr and Mn atoms are subjected to strong transverse displacive modulations correlated with the Cu site occupancy modulation. This analysis, however, also revealed that the sample was not single phase and was contaminated by a significant portion of the material from the less highly oxidized side of the phase gap. Subsequently, a smaller single phase sample (as judged by ID31 data) of the highly oxidized phase was synthesized and this was used for further analysis. Crystals of the highly oxidized material suitable for single crystal X-ray diffraction using a synchrotron source were extracted from powder samples and measured on the diffractometer I19 at the Diamond Light Source.

The XRSCD data from I19 together with the Rietveld analysis (Figure 1) of the single phase sample using ID31 data confirmed the model deduced from the initial powder diffraction experiment, and the structural modulation obtained from this analysis is represented in Figure 2(a). The refined parameters from the XRSCD experiment are included as supplementary material.[11] The modulated structure is derived from the body-centred tetragonal cell of the parent material (lattice parameters $a_T \sim 4.0$ Å and $c_T \sim 17.1$ Å) by a transformation to a face-centred orthorhombic cell with (at 100 K) $a_O = \sqrt{2}a_T = 5.6377(7)$ Å, $b_O = \sqrt{2}a_T = 5.6334(8)$ Å, and $c_O = c_T = 16.9735(16)$ Å, and this orthorhombic cell is then the basis for an incommensurately modulated structure with a modulation vector $\mathbf{q} = 0.2418\boldsymbol{a}_O^*$ corresponding to a modulation with a period in real space of about 23 Å along the a_O direction. The refinements reveal that the modulated occupancy of the tetrahedral Cu sites ranges between about 0.4 and 0.9 (Fig. S3)[11] with a mean value of 0.671(2) corresponding to a composition $Sr_2MnO_2Cu_{1.34(1)}S_2$ consistent with an extrapolation of the composition based on the cell volume. The oxide layers respond to the modulation of the Cu occupancy and a longitudinal (i.e., parallel to the modulation vector) modulation of the Cu position (Fig. S4)[11] by undergoing both longitudinal positional modulation and a larger transverse (perpendicular to the modulation vector) positional modulation, as is evident in Figure 2(a). This ensures that the sulfide ions do not become underbonded in the regions where the Cu content is rarefied. There are accordingly significant modulations in the Mn–S and Sr–S distances. Plots summarizing the modulation of the atomic positions and interatomic distances are provided as supplementary material (Figures S3–S13).[11]

Energy dispersive analysis of X-rays (EDX) on the single phase oxidized sample calibrated against a well-characterized[4] sample of composition $Sr_2MnO_2Cu_{1.5}S_2$ supported the composition deduced from the diffraction measurements producing elemental ratios: Sr2.00(5):Mn1.0(1):Cu1.27(13):S2.0(2). The room temperature High-Angle Annular Dark Field (HAADF)-STEM image (Figure 2(b)) taken freshly from this sample clearly shows the modulation evident from the analysis

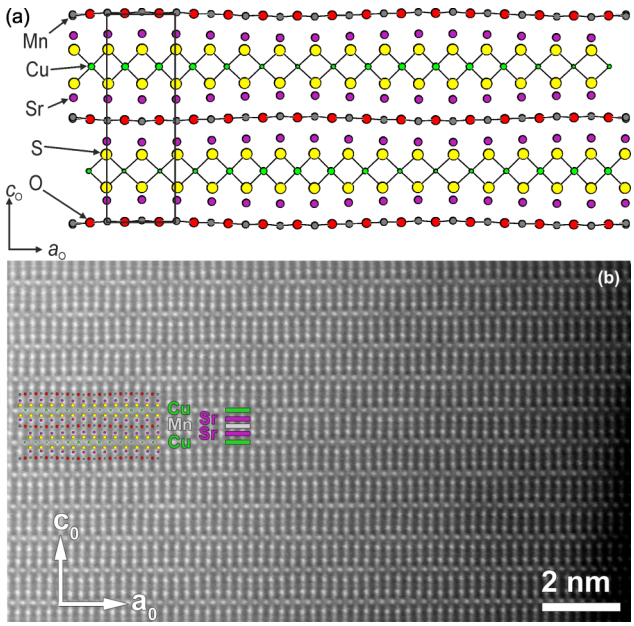

FIG. 2. (a) A representation of the modulated structure obtained from analysis of single crystal X-ray diffraction data. The occupational modulation of the Cu sites is depicted using the size of the green circles. The orthorhombic sub-cell $a_O \times b_O \times c_O$ which is the basis for the modulated structure is outlined. (b) The HAADF-STEM image along the same [010] projection as the model in (a). To indicate the nature of the different columns, the model is included as an overlap, and the cation layers have been indicated by coloured lines. The image has been corrected for drift during the scan and with a low band pass filter to reduce the noise.

of the diffraction data. The examination using this technique also revealed that over time the modulation became less obvious, presumably due to thermal decomposition in the electron beam.

Comparison of the Mn *K*-edge absorption of the parent and the single phase highly oxidized sample (Figure 3) showed a shift in the position of absorption edge of 0.30(5) eV consistent with the level of oxidation deduced from the composition obtained from EDX and the structure refinements. The Cu *K*-edge shift was 0.07(1) eV consistent with dominant oxidation of Mn. In these systems, oxidation of the Mn-3*d* states is anticipated until the point where the energy of these states has been lowered sufficiently that further oxidation results in oxidation of the Cu-3*d*/S-3*p* band. The relationship between crystal and electronic structure and the significance of the compositional phase gap in these compounds requires further elucidation.

Magnetic susceptibility measurements (Figure 3(a)) show the sensitivity of the systems to the electron count. The parent material $Sr_2MnO_2Cu_{1.5}S_2$ shows long range antiferromagnetic order below 30 K with the CE-type magnetic structure.[2,6] The most oxidized phase shows a broad magnetic transition at about 90 K and evidence at lower temperatures from the slight divergence of the zero-field-cooled and field-cooled susceptibilities, and the displacement of the hysteresis loop from the origin (Figure 3(a) inset) for a glassy component to the magnetism.

The analysis of the NPD data from D2B on the large sample used to derive the initial model for the oxidized phase confirmed the validity of the modulated structural model described above. The lower resolution of the diffractometer compared with ID31 did not enable the peaks of the second phase present in that sample to be resolved. The neutron diffractogram at 2 K (Figure 4) furthermore showed the presence of magnetic Bragg reflections which did not resemble either of the models (CE-type or A-type) found for the series $Sr_2MnO_2Cu_{1.5}(S_{1-x}Se_x)_2$[6] or a mixture of the two. The modelling of the magnetic reflections was enabled by the analysis of the magnetic scattering from the related oxidation product ($Sr_2MnO_2Cu_{3.3}S_3$) of the $m = 2$ member of the $Sr_2MnO_2Cu_{2m-\delta}S_{m+1}$ oxysulfide series.[4] This compound has a structural complexity that is still under investigation, but the magnetic scattering was indexed on a cell with a $\sqrt{2}a_T \times 3\sqrt{2}a_T$ basal plane expansion relative to the tetragonal structural subcell and a model containing two Mn sublattices was obtained

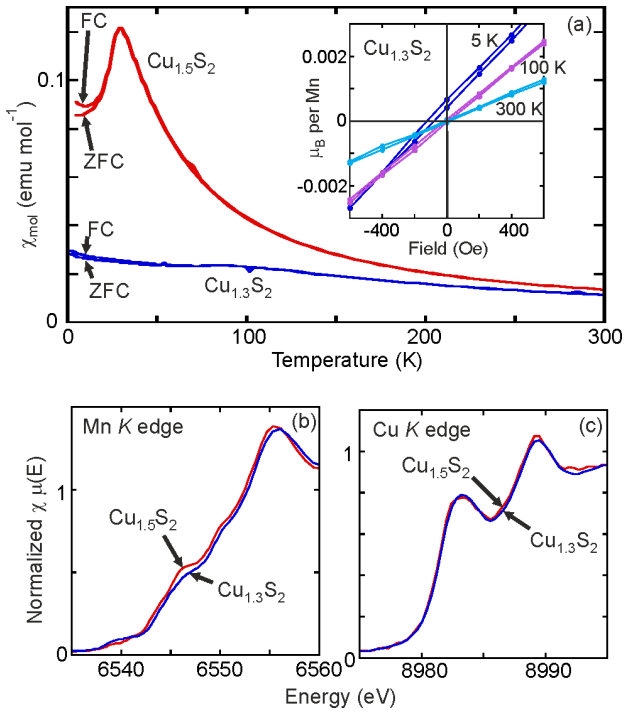

FIG. 3. (a) Evolution of the magnetic susceptibility on oxidation of $Sr_2MnO_2Cu_{1.5}S_2$ to $Sr_2MnO_2Cu_{1.3}S_2$. Inset: portions of field-cooled (5 T field) hysteresis loops for the oxidized sample. (b) The shift to higher energy of the Mn *K*-edge absorption compared with the much smaller shift of the Cu *K*-edge (c), showing that oxidation of Mn dominates.

from the intensities using the ISODISTORT software.[12] This model successfully accounted for the magnetic scattering in $Sr_2MnO_2Cu_{1.3}S_2$ and consists of ferromagnetic stripes coupled antiferromagnetically within the MnO_2 sheets. Refinement (Figure 4) against data from D2B using JANA2006[9] revealed similar moments of 3.8(1) μ_B for two distinct Mn sites. Control of the oxidation state of the

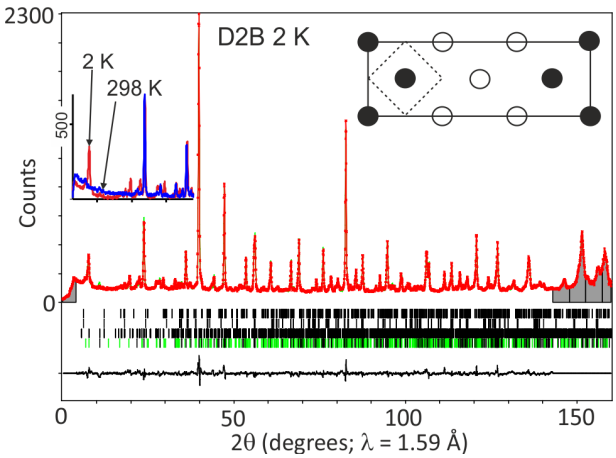

FIG. 4. Rietveld refinement against low temperature neutron diffraction data (D2B) using the Cu/vacancy modulated model deduced from electron and X-ray diffraction measurements on the same sample. Data (red), fit (green), and difference (lower black line) are shown. The shaded areas were excluded from the refinement. Tick marks are from bottom: modulated structural model for $Sr_2MnO_2Cu_{1.3}S_2$, magnetic model for $Sr_2MnO_2Cu_{1.3}S_2$, MnO nuclear phase, MnO magnetic phase. The left hand inset compares the low angle regions of the pattern at 298 K (blue) and 2 K (red) using the same horizontal scale as the main diagram; this shows the emergence of the main magnetic reflections. The right hand inset shows the magnetic structure modelled with Mn moments of 3.8(1) μ_B directed perpendicular to the MnO_2 sheets and directed into (filled circles) or out of (open circles) the plane. The dotted line depicts the basal unit cell dimensions for the ambient temperature tetragonal cell of the parent material ($a_T \times a_T$). The solid line depicts the cell used for the magnetic structure.

Mn ions in the oxide layers, by chemical deintercalation of copper ions from the sulfide layers, thus results in retention of long range magnetic order. But there are significant changes in the exchange interactions that result in the adoption of a new magnetic structure.

We have expanded the scope of layered oxide chalcogenide compounds using soft chemistry. The work suggests that further chemical and electrochemical approaches to the compositional modification of these mixed-valent transition metal systems will bear considerable fruit in tuning structural and physical properties. Here, we have demonstrated control over the structural features resulting from the ordering of mobile copper ions and vacancies and have shown the sensitivity of the magnetic properties to oxidation state in mixed-valent manganite oxide chalcogenides which are complementary to the much more extensively studied manganite oxides. While soft chemical techniques such as the oxidative deintercalation described here and reductive processes such as lithiation are well known to produce compositions that are metastable, they have the advantage that the electron count is controlled without dramatic change to the immediate chemical surroundings of the transition metal coordination sphere.

We thank the EPSRC for funding (Nos. EP/E025447 and EP/I017844) and the Diamond Light Source, Ltd., (DLS) for studentship support for S.J.C. (Cassidy) and J.N.B. We thank the ESTEEM2 network for enabling the electron microscopy investigations, and the DLS, the ILL, and the ESRF for awards of beamtime. We acknowledge the help of instrument scientists on I19 and B18 (G. Cibin) at DLS, M. Brunelli and E. Suard at ILL, and A. N. Fitch at ESRF.

[1] H. Hiramatsu, H. Yanagi, T. Kamiya, K. Ueda, M. Hirano, and H. Hosono, Chem. Mater. **20**, 326 (2008).
[2] S. J. Clarke, P. Adamson, S. J. C. Herkelrath, O. J. Rutt, D. R. Parker, M. J. Pitcher, and C. F. Smura, Inorg. Chem. **47**, 8473 (2008).
[3] C. F. Smura, D. R. Parker, M. Zbiri, M. R. Johnson, Z. A. Gál, and S. J. Clarke, J. Am. Chem. Soc. **133**, 2691 (2011).
[4] W. J. Zhu and P. H. Hor, J. Solid State Chem. **130**, 319 (1997).
[5] Z. A. Gál, O. J. Rutt, C. F. Smura, T. P. Overton, N. Barrier, S. J. Clarke, and J. Hadermann, J. Am. Chem. Soc. **128**, 8530 (2006).
[6] P. Adamson, J. Hadermann, C. F. Smura, O. J. Rutt, G. Hyett, D. G. Free, and S. J. Clarke, Chem. Mater. **24**, 2802 (2012).
[7] O. J. Rutt, G. R. Williams, and S. J. Clarke, Chem. Commun. **2006**, 2869.
[8] S. Indris, J. Cabana, O. J. Rutt, S. J. Clarke, and C. P. Grey, J. Am. Chem. Soc. **128**, 13354 (2006).
[9] V. Petricek, M. Dusek, and L. Palatinus, Z. Kristallogr. **229**(5), 345 (2014).
[10] P. Adamson, Ph.D. thesis, University of Oxford, 2010.
[11] See supplementary material at http://dx.doi.org/10.1063/1.4918973 for details of structural refinements bond length data.
[12] ISOTROPY Software Suite iso.byu.edu; B. J. Campbell, H. T. Stokes, D. E. Tanner, and D. M. Hatch, J. Appl. Cryst. **39**, 607 (2006).